

On the extraction of the intrinsic light-quark sea in the proton

Wen-Chen Chang (章文箴)

Institute of Physics, Academia Sinica, Taipei 11529, Taiwan

Jen-Chieh Peng (彭仁傑)

Department of Physics, University of Illinois at Urbana-Champaign, Urbana, Illinois 61801, USA

Abstract

The HERMES collaboration recently reported a reevaluation of the strange-quark parton distribution, $S(x)$, based on kaon production in semi-inclusive deep-inelastic scattering. Two distinct results on $S(x)$ at the $x > 0.1$ region, one with a sizable magnitude and another with a vanishing content, were reported. We show that the latter result is due to a particular assumption adopted in the analysis. The impact of the new HERMES $S(x)$ result on the extraction of intrinsic light-quark sea in the proton is discussed. Given the large uncertainty in the kaon fragmentation function, we find that the latest HERMES data do not exclude the existence of a significant intrinsic strange-quark sea in the proton. The x dependence of the $(s + \bar{s})/(\bar{u} + \bar{d})$ ratio is also in qualitative agreement with the presence of intrinsic strange-quark sea.

I. INTRODUCTION

The large magnitude of the coupling constant, α_s , in strong interaction implies that sea quarks, like valence quarks and gluons, represent an integral part of the nucleon's structure. Unlike the valence quarks in the nucleons, which are restricted to the u and d , the sea quarks can have any quark flavors. This leads to a potentially rich flavor structure for the nucleon sea and could offer new insights on the nucleon structure. While decades of experimental and theoretical work has focused on the valence quark distributions, many important properties of the sea quarks, including their flavor, spin, and momentum dependencies, remain to be better determined.

A major surprise in the flavor structure of the nucleon sea was found when deep-inelastic scattering (DIS) and Drell-Yan experiments showed that the \bar{u} and \bar{d} in the proton have strikingly different Bjorken- x dependence [1–6]. Theoretical models which can explain this flavor asymmetry also have specific predictions on other aspects of spin and flavor structures of sea quarks. For example, the $s(x)$ and $\bar{s}(x)$ distributions are predicted to be different in, e.g., the meson cloud model [7, 8], the statistical model [9, 10], and the chiral soliton model [11]. It is also interesting to investigate how the flavor asymmetry between \bar{u} and \bar{d} is extended to the SU(3) case when the s and \bar{s} seas are included.

Our knowledge on the strange quark contents in the nucleons comes primarily from neutrino DIS and charged-lepton semi-inclusive DIS (SIDIS) experiments. From neutrino DIS, the momentum fraction carried by $s + \bar{s}$, integrated over the measured x range, is found to be roughly half of that carried by the lighter $\bar{u} + \bar{d}$ quarks [12, 13], reflecting a broken SU(3) symmetry for the proton's sea. In 2008, the HERMES collaboration reported a determination of $x(s(x) + \bar{s}(x))$ over the range of $0.02 < x < 0.5$ at $Q^2 = 2.5 \text{ GeV}^2$ from their measurement of SIDIS for charged-kaon production on a deuteron target with e^\pm beam [14]. The invariant mass of the photon-nucleon system W is required to be greater than $\sqrt{10} \text{ GeV}$. The HERMES result shows an intriguing feature that $x(s(x) + \bar{s}(x))$ for $x < 0.1$ rises rapidly with decreasing x , becoming comparable to $x(\bar{u}(x) + \bar{d}(x))$ from the CTEQ6L parton distribution function (PDF) [15] at $x < 0.05$. The Fermilab E866 Drell-Yan experiment also shows that the $\bar{d}(x)/\bar{u}(x)$ ratio approaches unity at the lowest value of x (~ 0.02) [16]. These results suggest the presence of an SU(3) flavor symmetric proton sea in the small- x region. Recently, the ATLAS collaboration determined the strange-to-down sea-quark ratio $r_s (\equiv (s + \bar{s})/2\bar{d})$ to be $1.00^{+0.25}_{-0.28}$ at $x = 0.023$ and $Q^2 = 1.9 \text{ GeV}^2$ from an analysis of inclusive W and Z boson production in pp collisions at 7 TeV [17]. Furthermore, the ATLAS col-

laboration determined the same ratio r_s to be $0.96^{+0.26}_{-0.30}$ at $Q^2=1.9 \text{ GeV}^2$ from their measurement of the associated $W+c$ production at LHC [18]. These results strongly suggests an SU(3)-symmetric light-quark sea, i.e., $\bar{u} = \bar{d} = \bar{s}$, in the small- x region. Results from HERMES, ATLAS, as well as the earlier neutrino results, imply a strong x dependence for the $[s(x) + \bar{s}(x)]/[\bar{u}(x) + \bar{d}(x)]$ ratio.

Another intriguing aspect of the nucleon sea is the concept of “intrinsic” sea, suggested by Brodsky, Hoyer, Peterson, and Sakai (BHPS) [19] to explain the enhanced production rates for charmed hadrons in the forward rapidity region. The $c\bar{c}$ component in the $|uudc\bar{c}\rangle$ is called the “intrinsic” sea in order to distinguish it from the conventional “extrinsic” sea originating from the $g \rightarrow c\bar{c}$ QCD process. The intrinsic sea is predicted to have a valence-like momentum distribution peaking at relatively large x . This is in contrast to the extrinsic sea, which dominates in the small- x region due to gluon splitting. Recently, the concept of intrinsic charm was generalized to the light-quark sector [20]. Since the probability for the $|uudQ\bar{Q}\rangle$ Fock state is expected to be roughly proportional to $1/m_Q^2$, where m_Q is the mass of quark Q , these light-quark intrinsic seas should be more abundant than the intrinsic charm quark. Using the kaon SIDIS data from HERMES on $s(x) + \bar{s}(x)$ [14], the E866 Drell-Yan data on $\bar{d}(x) - \bar{u}(x)$ [16], and the CTEQ6.6 PDF [21], it was shown that the probabilities for the $|uudu\bar{u}\rangle$, $|uudd\bar{d}\rangle$, and $|uuds\bar{s}\rangle$ Fock states have been extracted, supporting the existence of the intrinsic light-quark sea [20].

Recently, the HERMES collaboration reported the latest result on charged-kaon multiplicities where a multi-dimensional unfolding procedure was performed [22]. This led to a reevaluation of the strange-quark distributions, $S(x) \equiv s(x) + \bar{s}(x)$ [23]. Depending on the kaon fragmentation function adopted in the analysis, two distinct results, corresponding to significantly different $S(x)$ at the $x > 0.1$ region, were obtained by the HERMES collaboration [23]. Since the HERMES result on $S(x)$ is a crucial input for the extraction of the intrinsic light-quark sea, we have extended our previous analysis [20] to take into account the latest HERMES results. In this paper, we first discuss the uncertainties in the extraction of $S(x)$ associated with the uncertainty in the kaon fragmentation functions which are still poorly known. We then recapitulate the procedure to extract the intrinsic sea in the BHPS model and present the updated results on the extraction of the intrinsic light-quark sea using several different assumptions for the kaon fragmentation functions. The x dependence of the $(s(x) + \bar{s}(x))/(\bar{u}(x) + \bar{d}(x))$ ratio is also discussed in the context of the extrinsic and intrinsic seas.

II. EXTRACTION OF $S(x)$ FROM HERMES KAON SIDIS DATA

The HERMES collaboration extracted $S(x)$ from the spin-averaged kaon multiplicity, $dN^K(x, Q^2)/dN^{DIS}(x, Q^2)$, measured with 27.6 GeV positrons or electrons scattered off a deuterium target in the DIS region [22]. The HERMES $dN^K(x, Q^2)/dN^{DIS}(x, Q^2)$ data are shown in Fig. 1(a). For the isoscalar deuteron nucleus, the kaon multiplicity is expressed in leading order as follows [14, 23]:

$$\frac{dN^K(x, Q^2)}{dN^{DIS}(x, Q^2)} = \frac{Q(x, Q^2) \int_{0.2}^{0.8} D_Q^K(z, Q^2) dz + S(x, Q^2) \int_{0.2}^{0.8} D_S^K(z, Q^2) dz}{5Q(x, Q^2) + 2S(x, Q^2)} \quad (1)$$

where $S(x, Q^2) \equiv s(x, Q^2) + \bar{s}(x, Q^2)$ and $Q(x, Q^2) \equiv u(x, Q^2) + \bar{u}(x, Q^2) + d(x, Q^2) + \bar{d}(x, Q^2)$. The $D_S^K(z, Q^2)$ and $D_Q^K(z, Q^2)$ are their corresponding fragmentation functions for hadronizing into charged kaons. The values of 0.2 and 0.8 are the lower and upper limits of the variable $z = E_K/\nu$, where ν and E_K are the energies of the virtual photon and the kaon in the target rest frame, respectively. Eq. (1) can be rearranged as

$$S(x, Q^2) = \frac{Q(x, Q^2) [5(\frac{dN^K(x, Q^2)}{dN^{DIS}(x, Q^2)}) - \int_{0.2}^{0.8} D_Q^K(z, Q^2) dz]}{\int_{0.2}^{0.8} D_S^K(z, Q^2) dz - 2(\frac{dN^K(x, Q^2)}{dN^{DIS}(x, Q^2)})}. \quad (2)$$

Eq. (2) shows that $S(x, Q^2)$ can be directly evaluated by using the HERMES kaon multiplicity data, the values of $Q(x, Q^2)$ from recent PDFs, and $D_Q^K(z, Q^2)$, $D_S^K(z, Q^2)$ from the latest parametrization of kaon fragmentation functions (FF). The result of $xS(x)$ for an evaluation using the CTEQ6L PDF [15] and the DSS FF [24] are shown in Fig. 2 of Ref. [23] and as “HERMES2014-set1” in Fig. 1(b) (statistical errors only). For the $0.03 < x < 0.2$ range, the extracted $xS(x)$ values are much larger than what are predicted by CTEQ6L PDF but closer to those of CTEQ6.5S-0 [25], a reference PDF set with unconstrained $xS(x)$ shape. For the three largest x points at $x > 0.2$, the extracted $xS(x)$ values are larger than the PDF values, although the differences are comparable to the large systematic uncertainties estimated by the HERMES collaboration [23].

An alternative approach was adopted by the HERMES collaboration where the integral $\int_{0.2}^{0.8} D_Q^K(z, Q^2) dz$ was estimated using their kaon multiplicity data. Eq. (1) could be rearranged as

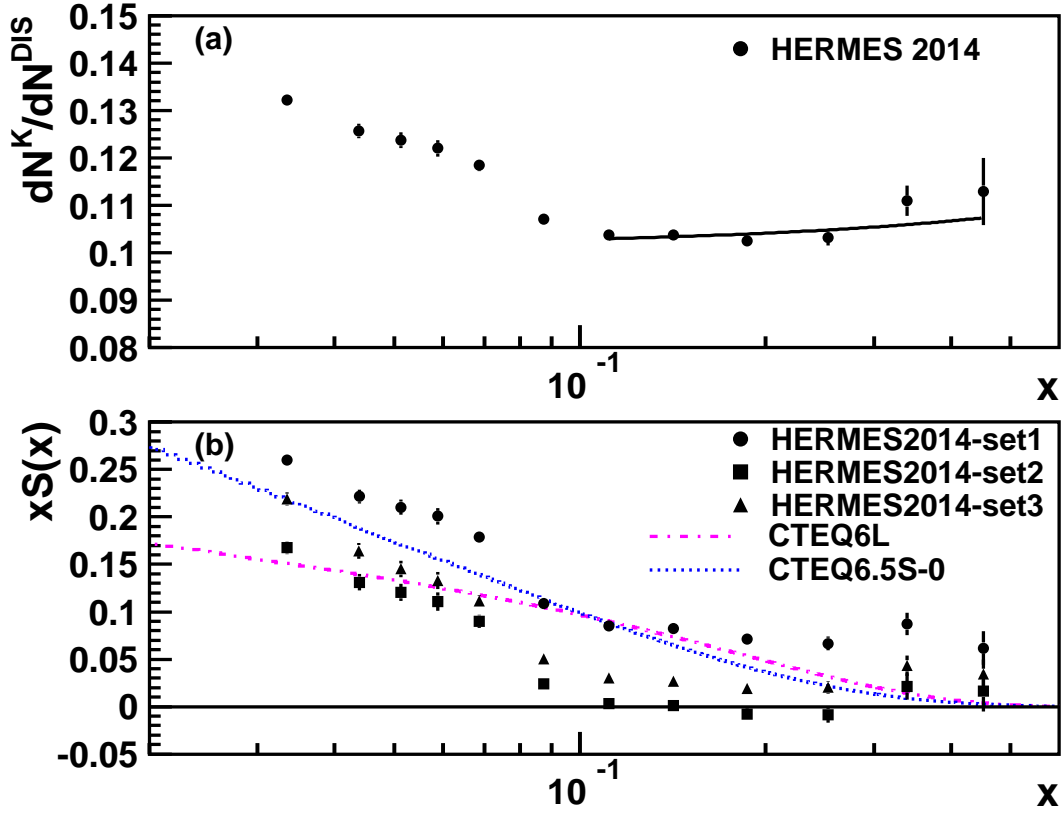


FIG. 1: (a) The fit to the $dN^K/dN^{DIS}(x, Q^2)$ HERMES data [23] (solid circles) for the determination of an effective value of $\int D_Q^K(z, Q^2)dz$. (b) The strange parton distribution $xS(x)$ determined from the measured charged-kaon multiplicities shown in the Fig. 2 (HERMES2014-set1) and Fig. 4 (HERMES2014-set2) of Ref. [23]. Also shown is the $xS(x)$ distribution of HERMES2014-set3, described in the text. For clarity, only statistics errors are shown. Systematic uncertainties are available in Ref. [23].

$$\int_{0.2}^{0.8} D_Q^K(z, Q^2)dz = 5 \frac{dN^K(x, Q^2)}{dN^{DIS}(x, Q^2)} - \frac{S(x, Q^2)}{Q(x, Q^2)} \left[\int_{0.2}^{0.8} D_S^K(z, Q^2)dz - 2 \frac{dN^K(x, Q^2)}{dN^{DIS}(x, Q^2)} \right]. \quad (3)$$

When $S(x, Q^2)/Q(x, Q^2)$ is sufficiently small, the second term on the RHS of Eq. (3) can be neglected with respect to the first term, and Eq. (3) simplifies to

$$\int_{0.2}^{0.8} D_Q^K(z, Q^2)dz = 5 \frac{dN^K(x, Q^2)}{dN^{DIS}(x, Q^2)}. \quad (4)$$

Eq. (4) has the property that the LHS is independent of x , while the RHS is potentially a func-

tion of x . For the x region in which this equation is valid, the RHS must be independent of x . Interestingly, the HERMES data on $dN^K(x, Q^2)/dN^{DIS}(x, Q^2)$ are consistent with having a flat x dependence for $x > 0.1$, suggesting the validity of Eq. (4) in the $x > 0.1$ region. The HERMES collaboration obtained a linear fit to the $dN^K(x, Q^2)/dN^{DIS}(x, Q^2)$ data at $x > 0.1$ as $dN^K(x, Q^2)/dN^{DIS}(x, Q^2) = (0.102 \pm 0.002) + (0.013 \pm 0.010)x$, shown as the curve in Fig. 1(a). This corresponds to a value of $\int_{0.2}^{0.8} D_Q^K(z, Q^2) dz = 5dN^K(x, Q^2)/dN^{DIS}(x, Q^2) = 0.514 \pm 0.010$ at $Q^2 = 2.5 \text{ GeV}^2$ using Eq. (4) (note that at $x = 0.13$, $Q^2 \sim 2.5 \text{ GeV}^2$ for the HERMES data). From this determination of $\int_{0.2}^{0.8} D_Q^K(z, Q^2) dz$, together with $Q(x, Q^2)$ from the CTEQ6L PDF [15] and $D_S^K(z, Q^2)$ from the DSS FF [24], $S(x, Q^2)$ can be readily obtained using Eq. (2). The slight Q^2 -dependence for $D_Q^K(z, Q^2)$ was taken into account by the same scale dependence as the DSS FF. The extracted $S(x)$ at $Q^2 = 2.5 \text{ GeV}^2$ with statistical errors only, shown as “HERMES2014-set2” in Fig. 1(b), largely vanishes for $x > 0.1$, which reflects the assumption used in this approach. In particular, Eqs. (3) and (4) ensure that $S(x) \rightarrow 0$ for $x > 0.1$, where the validity of Eq. (4) is assumed by HERMES [23]. This striking result of vanishing $S(x)$ at $x > 0.1$ is at variance with all existing PDFs, including CTEQ6L and CTEQ6.5S-0 shown in Fig. 1(b).

The method of extracting $\int_{0.2}^{0.8} D_Q^K(z, Q^2) dz$ from the HERMES kaon multiplicity data is interesting, but it does not take into account the constraints provided by the bulk of existing e^+e^- and SIDIS data. As discussed earlier, a straightforward approach to extract $S(x)$ from the HERMES data is to use the DSS kaon fragmentation functions of $D_Q^K(z, Q^2)$ and $D_S^K(z, Q^2)$ from the latest global fit to extensive data sets [24]. Note that the DSS FF gives $\int_{0.2}^{0.8} D_Q^K(z, Q^2) dz = 0.435$ at $Q^2 = 2.5 \text{ GeV}^2$, which is $\sim 20\%$ smaller than the HERMES result. Adopting this value from the DSS FF in Eq. (2), there is room for non-zero values of $S(x)$ at $x > 0.1$, since $5(dN^K(x, Q^2)/dN^{DIS}(x, Q^2))$ is now greater than $\int_{0.2}^{0.8} D_Q^K(z, Q^2) dz$. This would also lead to larger values of $xS(x)$ in the small- x region, as shown as “HERMES2014-set2” (statistic errors only) in Fig. 1(b) (square points).

It is important to note that a flat x dependence for $dN^K(x, Q^2)/dN^{DIS}(x, Q^2)$ data at $x > 0.1$ does not ensure the validity of Eq. (4). Indeed, it is plausible that the second term on the RHS of Eq. (3) can contribute on the order of several percents relative to the first term. This would lower the value of $\int_{0.2}^{0.8} D_Q^K(z, Q^2) dz$ and the extracted $S(x)$ would be larger than the “HERMES2014-set2” result in Fig. 1(b). To assess the relative importance of the second term on the RHS of Eq. (3), we have investigated the contribution of this term to Eq. (3) using a variety of PDFs. We found that the ratios of the second term to the first term on the RHS of Eq. (3) at $x = 0.25$, which

is near the mean x value of the HERMES data at the $x > 0.1$ region, are 6.2%, 3.5% and 4.4% for CTEQ6L [15], NNPDF2.3L [26] and MMHT2014L [27] respectively. We extracted the values of $xS(x)$ from the HERMES kaon multiplicity data following the same procedure taking into account the finiteness of the second term on the RHS of Eq. (3). The results by setting the ratios of the second term to the first term on the RHS of Eq. (3) to be the average value 4.8% are shown as “HERMES2014-set3” (statistical errors only) in Fig. 1(b) (triangular points). We note that the problems encountered by the other two approaches, namely the large $S(x)$ content at $x > 0.2$ in HERMES2014-set1, or the vanishing strange-quark content at $x > 0.1$ in HERMES2014-set2, are largely mitigated.

In the rest of this paper, we present the results on the extraction of the intrinsic strange and non-strange sea by using the two results of $S(x)$ obtained by HERMES [23] together with the “HERMES2014-set3” result. For comparison, we also include the result using the values of $S(x)$ from the earlier HERMES publication [14]. The goal of this study is to assess the range of uncertainty in the extraction of the light-quark intrinsic sea, resulting from the uncertainty in $S(x)$ extracted from the HERMES data. Table I summarizes the label, extraction method and reference information for each $S(x)$ data set to be studied.

Label	Method	Reference
HERMES2008	Eq. 2 and Eq. 4	Ref. [14]
HERMES2014-set1	Eq. 2 and DSS FF	Ref. [23], Fig. 2
HERMES2014-set2	Eq. 2 and Eq. 4	Ref. [23], Fig. 4
HERMES2014-set3	Eq. 2 and Eq. 3	

TABLE I: The label, extraction method and reference for each $S(x)$ data set.

III. EXTRACTION OF INTRINSIC LIGHT-QUARK SEAS

In the BHPS model [19], the probability of the $|uudQ\bar{Q}\rangle$ proton five-quark Fock state, where quark i carries a momentum fraction x_i , is given as

$$P(x_1, \dots, x_5) = N_5 \delta(1 - \sum_{i=1}^5 x_i) [m_p^2 - \sum_{i=1}^5 \frac{m_i^2}{x_i}]^{-2}, \quad (5)$$

where the delta function ensures momentum conservation. N_5 is the normalization factor, and m_i is the mass of quark i . The last two quarks ($i = 4, 5$) refer to intrinsic sea quark pair $Q\bar{Q}$ in the five-quark Fock state. The momentum distribution, $P(x_i)$, for quark i is obtained by integrating Eq. (5) over the momentum fractions of the remaining quarks. An analytical expression for the probability distribution $P(x_5)$ for \bar{Q} is available [19] in the limit of $m_{4,5} \gg m_p, m_{1,2,3}$. When Q is the lighter u, d , or s quark, for which one could no longer assume a large mass, we developed the algorithm to calculate $P(x_5)$ according to Eq. (5) with Monte-Carlo techniques [20], and $m_u = m_d = 0.3 \text{ GeV}/c^2$, $m_s = 0.5 \text{ GeV}/c^2$, and $m_p = 0.938 \text{ GeV}/c^2$.

The challenge for identifying the intrinsic seas is to separate them from the much more abundant extrinsic seas. Two approaches were considered [20]. The first is to select experimental observables which have little or no contributions from the extrinsic seas. The $\bar{d}(x) - \bar{u}(x)$, which was measured in a Drell-Yan experiment [16], is an example of flavor-nonsinglet quantities which are largely free from the contributions of the extrinsic sea quarks, since the perturbative $g \rightarrow Q\bar{Q}$ processes will generate $u\bar{u}$ and $d\bar{d}$ pairs with very similar probabilities and have little or no contribution to this quantity. Another example for the quantities largely free from the extrinsic sea is the SU(3) flavor-nonsinglet $\bar{u}(x) + \bar{d}(x) - s(x) - \bar{s}(x)$ distribution, which is obtained from the HERMES data on $s(x) + \bar{s}(x)$ together with $\bar{u}(x) + \bar{d}(x)$ from PDF global analysis.

The second approach is to rely on their different x dependencies. As mentioned earlier, the extrinsic sea is more abundant in the small- x region while the intrinsic sea is valence-like and is dominant in the large- x region. The HERMES $S(x)$ data in Ref. [14] showed an intriguing feature of a sharp rise towards small x ($x < 0.1$) and a broad structure in the larger x region. This suggests the presence of two distinct components of the strange sea, an extrinsic part dominating at small x and an intrinsic component in the $x > 0.1$ region. A comparison between the HERMES data and the calculations using the BHPS model showed good agreement [20], supporting the interpretation that the data at $x > 0.1$ have a significant contribution from the intrinsic sea.

The moment of $P(x_5)$ is defined as $\mathcal{P}_5^{Q\bar{Q}} (\equiv \int_0^1 P(x_5) dx_5)$ and represents the probability of the $|uudQ\bar{Q}\rangle$ five-quark Fock state in the proton. We take the same approach as described in Ref. [20] to extract the five-quark components of the proton, $\mathcal{P}_5^{u\bar{u}}$, $\mathcal{P}_5^{d\bar{d}}$ and $\mathcal{P}_5^{s\bar{s}}$. First, the difference $\mathcal{P}_5^{d\bar{d}} - \mathcal{P}_5^{u\bar{u}}$ was constrained to be 0.118 ± 0.012 by the normalization of $\bar{d}(x) - \bar{u}(x)$ from the measurement of Fermilab E866 Drell-Yan experiment [16]. The $\mathcal{P}_5^{s\bar{s}}$ is obtained from four different sets of data for $xS(x)$ at $x > 0.1$ and $Q^2 = 2.5 \text{ GeV}^2$: HERMES2008, HERMES2014-set1, HERMES2014-set2, and HERMES2014-set3, respectively. The total errors of $xS(x)$ obtained by the square-root

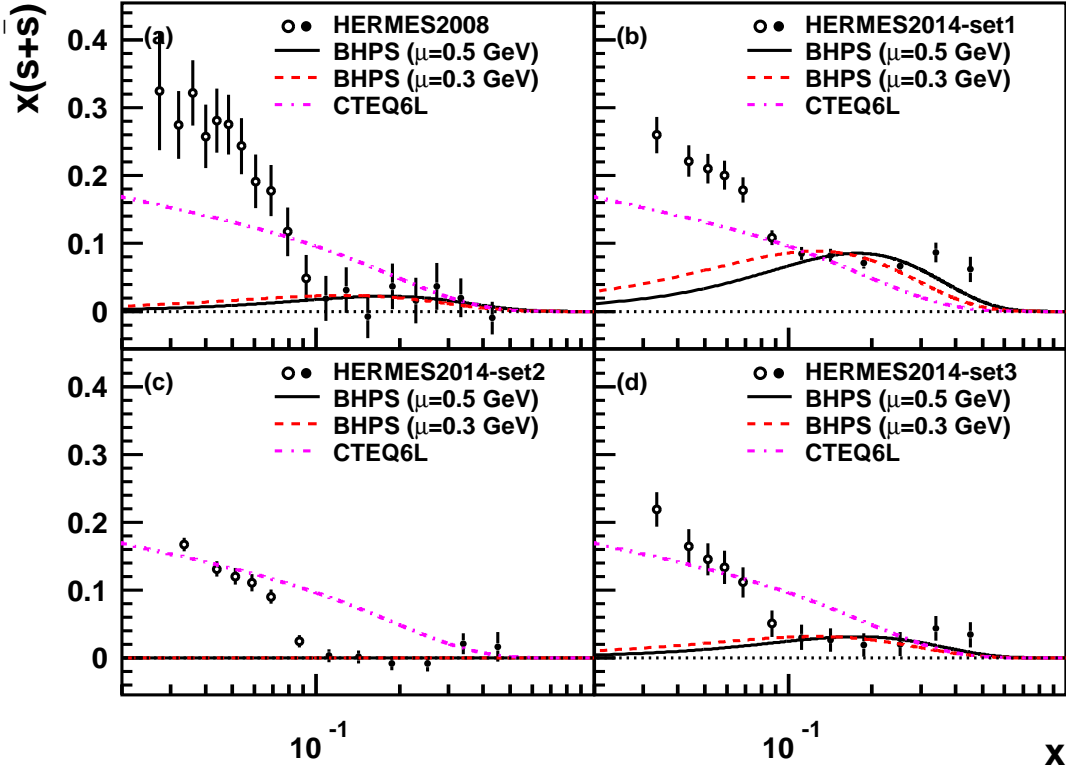


FIG. 2: Comparison of the HERMES $x(s(x) + \bar{s}(x))$ data with the calculations based on the BHPs model. The solid black and dashed red curves are obtained by evolving the BHPs result to $Q^2 = 2.5 \text{ GeV}^2$ using the initial scale $\mu = 0.5 \text{ GeV}$ and $\mu = 0.3 \text{ GeV}$, respectively. The normalizations of the calculations are adjusted to fit the data at $x > 0.1$, denoted by solid circles. The blue dash-dot and dotted lines denote the $x(s(x) + \bar{s}(x))$ from CTEQ6L [15] and CTEQ6.5S-0 [25], respectively. The labels (a), (b), (c) and (d) denote the different inputs of $xS(x)$ from HERMES2008, HERMES2014-set1, HERMES2014-set2 and HERMES2014-set3.

sum of the statistical and systematic errors are used in the analysis. Figure 2 shows the fit to $xS(x)$ at $x > 0.1$ using the BHPs model to extract the intrinsic sea for these four sets of data. The solid and dashed curves are obtained by evolving the BHPs result to $Q^2 = 2.5 \text{ GeV}^2$ using the initial scale value of $\mu = 0.5 \text{ GeV}$ and $\mu = 0.3 \text{ GeV}$, respectively. The normalization of the calculations are adjusted to fit the data at $x > 0.1$. The $xS(x)$ from CTEQ6L [15] and CTEQ6.5S-0 [25] are also shown.

Combining the HERMES data on $x(s(x) + \bar{s}(x))$ with the $x(\bar{d}(x) + \bar{u}(x))$ distributions determined from the global analysis of CTEQ6.6 [21], the quantity $x(\bar{u}(x) + \bar{d}(x) - s(x) - \bar{s}(x))$ can be

obtained and compared with the calculation of the intrinsic sea in the BHPS model for the determination of $\mathcal{P}_5^{u\bar{u}} + \mathcal{P}_5^{d\bar{d}} - 2\mathcal{P}_5^{s\bar{s}}$. Figure 3 shows the comparison of $x(\bar{u}(x) + \bar{d}(x) - s(x) - \bar{s}(x))$ with the calculations based on the BHPS model. The solid black and dashed red curves are obtained by evolving the BHPS result to $Q^2 = 2.5 \text{ GeV}^2$ using $\mu = 0.5 \text{ GeV}$ and $\mu = 0.3 \text{ GeV}$, respectively.

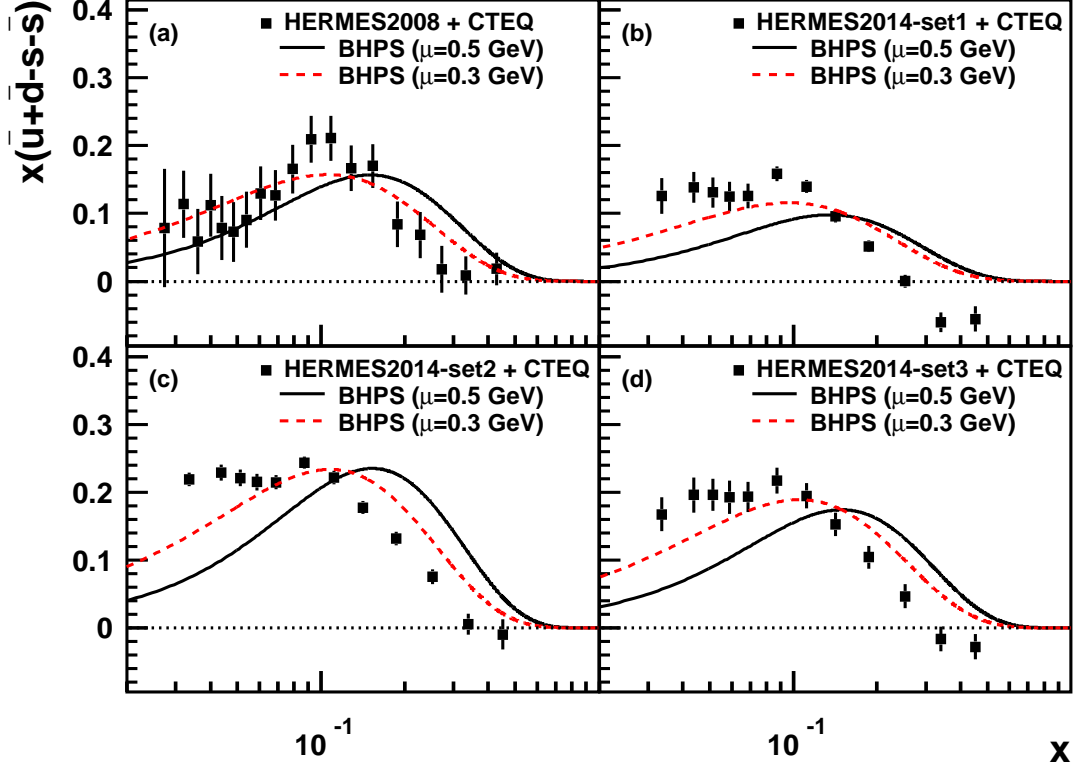


FIG. 3: Comparison of the $x(\bar{u}(x) + \bar{d}(x) - s(x) - \bar{s}(x))$ with the calculations based on the BHPS model. The solid black and dashed red curves are obtained by evolving the BHPS result to $Q^2 = 2.5 \text{ GeV}^2$ using $\mu = 0.5 \text{ GeV}$ and $\mu = 0.3 \text{ GeV}$, respectively. The normalizations of the calculations are adjusted to fit the data. The labels (a), (b), (c) and (d) denote the different inputs of $xS(x)$ from HERMES2008, HERMES2014-set1, HERMES-set2 and HERMES-set3.

Putting these three quantities together we can determine the probabilities $\mathcal{P}_5^{u\bar{u}}$, $\mathcal{P}_5^{d\bar{d}}$ and $\mathcal{P}_5^{s\bar{s}}$ for the $|uud\bar{u}\bar{u}\rangle$, $|uudd\bar{d}\rangle$, and $|uuds\bar{s}\rangle$ configurations individually. The extracted $\mathcal{P}_5^{u\bar{u}}$, $\mathcal{P}_5^{d\bar{d}}$ and $\mathcal{P}_5^{s\bar{s}}$, from four sets of data (HERMES2008, HERMES2014-set1, HERMES2014-set2 and HERMES2014-set3) are listed in Table II. Since the $s + \bar{s}$ were extracted using a LO analysis of the HERMES data, we have also performed analyses using the LO CTEQ6.5S-0 [25] and CTEQ6L [15] PDFs in addition to the NLO CTEQ6.6 [21] PDF. The results of $\mathcal{P}_5^{u\bar{u}}$ and $\mathcal{P}_5^{d\bar{d}}$

are shown in parentheses. Table II shows that the extracted values of $\mathcal{P}_5^{s\bar{s}}$, varying from zero to ~ 0.11 , depends sensitively on the choice of $S(x)$. It is interesting to note that the values of $\mathcal{P}_5^{s\bar{s}}$ extracted [6] using the HERMES2008 data are closest to those obtained with the HERMES2014-set3. Table II also shows that the values of $\mathcal{P}_5^{u\bar{u}}$ and $\mathcal{P}_5^{d\bar{d}}$ are relatively insensitive to the choice of $S(x)$. Finally, the results have only minor dependence on the choice of the PDF.

$xS(x)$	μ (GeV)	$\mathcal{P}_5^{u\bar{u}}$	$\mathcal{P}_5^{d\bar{d}}$	$\mathcal{P}_5^{s\bar{s}}$
HERMES2008	0.5	0.120 (0.128, 0.112)	0.238 (0.246, 0.230)	0.022
HERMES2008	0.3	0.161 (0.174, 0.145)	0.279 (0.292, 0.263)	0.029
HERMES2014-set1	0.5	0.125 (0.131, 0.124)	0.243 (0.249, 0.242)	0.086
HERMES2014-set1	0.3	0.194 (0.202, 0.188)	0.312 (0.320, 0.306)	0.111
HERMES2014-set2	0.5	0.178 (0.187, 0.167)	0.296 (0.305, 0.285)	0.000
HERMES2014-set2	0.3	0.229 (0.242, 0.211)	0.347 (0.360, 0.329)	0.000
HERMES2014-set3	0.5	0.148 (0.156, 0.142)	0.266 (0.274, 0.260)	0.031
HERMES2014-set3	0.3	0.213 (0.225, 0.200)	0.331 (0.343, 0.318)	0.039

TABLE II: The extracted values of $\mathcal{P}_5^{u\bar{u}}$, $\mathcal{P}_5^{d\bar{d}}$ and $\mathcal{P}_5^{s\bar{s}}$ from E866 [16], CTEQ6.6 [21] and four sets of HERMES's data (HERMES2008, HERMES2014-set1, HERMES2014-set2 and HERMES2014-set3) assuming two initial scales (μ) for the BHPS five-quark distributions. The results of $\mathcal{P}_5^{u\bar{u}}$ and $\mathcal{P}_5^{d\bar{d}}$ using CTEQ6.5S-0 [25] and CTEQ6L [15] PDFs are also shown in parentheses.

IV. DISCUSSION

The intrinsic five-quark strange component $\mathcal{P}_5^{s\bar{s}}$ in the BHPS model is connected with the size of $xS(x)$ in valence-like, i.e. large- x region. The value of $\mathcal{P}_5^{s\bar{s}}$ is about 2-3% for the HERMES2008 data [14] and is either reduced to less than 0.1% or enhanced to 8-10% depending on the choice of the data sets. In Fig. 4 we compare the HERMES's SIDIS results of $xS(x)$ distributions at $Q^2 = 2.5 \text{ GeV}^2$ with the CCFR's results at $Q^2 = 1 \text{ GeV}^2$ and 4 GeV^2 [12]. The distributions of $xS(x)$ at $Q^2 = 2.5 \text{ GeV}^2$ from CTEQ6L [15], NNPDF2.3L [26] and MMHT2014L [27] leading-order PDFs are overlaid. The assumption of vanishing strangeness for $x > 0.1$, adopted in the recent HERMES's analysis, leads to results clearly at odds with the data from the neutrino DIS

experiment and the results of all PDFs. Overall, the results using DSS FF (“HERMES2014-set1”) agree best with the CCFR Data. Table II shows that the value of $P_5^{s\bar{s}}$ is of the order of 0.03 to 0.11 from HERMES2014-set2 and HERMES2014-set3. A reliable extraction of $xS(x)$ and $P_5^{s\bar{s}}$ would require a more precise knowledge on the kaon fragmentation functions [28], and a new global fit taking into account the recent HERMES [22] and COMPASS [29] kaon SIDIS data would be most valuable.

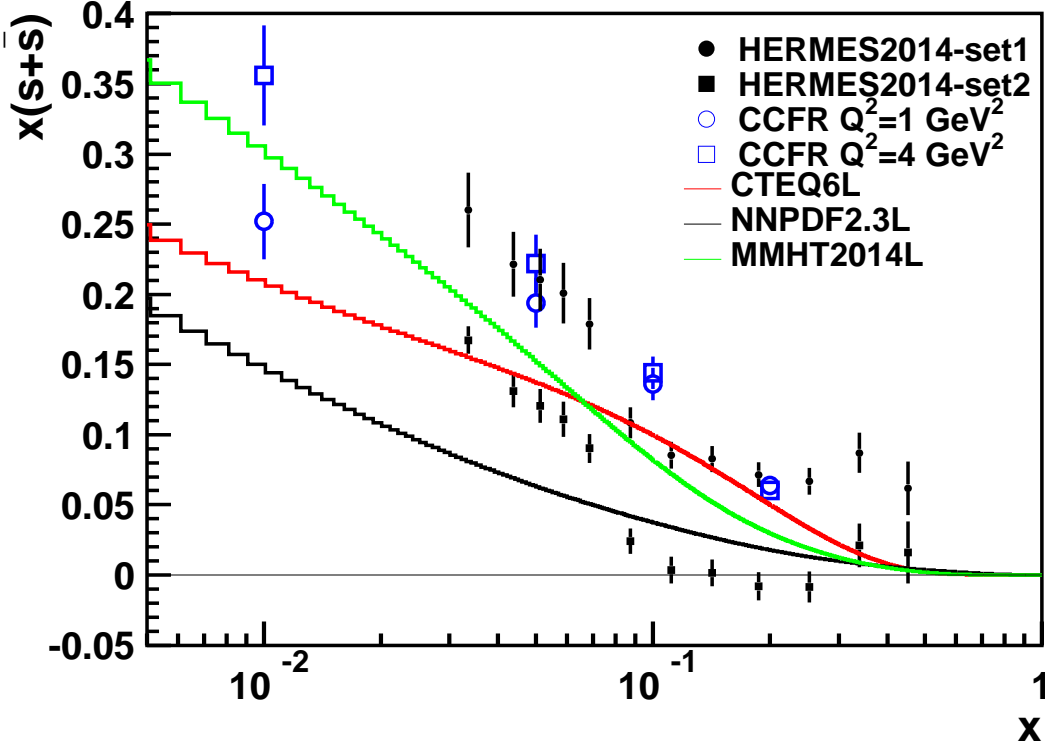


FIG. 4: The strange parton distribution $x(s + \bar{s})$ from HERMES2014-set1 and HERMES2014-set2 (statistical errors only) at $Q^2 = 2.5 \text{ GeV}^2$, compared with those of CCFR (including statistical and systematic errors) at $Q^2 = 1 \text{ GeV}^2$ and 4 GeV^2 [12]. The $x(s + \bar{s})$ from three leading-order PDFs, CTEQ6L [15], NNPDF2.3L [26] and MMHT2014L [27], are overlaid.

Figure 5 shows the ratio of strange-to-nonstrange sea quarks $(s + \bar{s})/(\bar{u} + \bar{d})$ as a function of x using the HERMES data of $(s + \bar{s})$ and the $(\bar{u} + \bar{d})$ from CTEQ6L [15] at $Q^2 = 2.5 \text{ GeV}^2$. There are two observations for the ratios: an enhancement at large x and a rise towards 1 at very small x . The first observation is consistent with the existence of intrinsic strange sea which is distributed in larger x region relative to the intrinsic non-strange one because $m_s > m_{u,d}$. The second observation suggests the presence of SU(3) flavor symmetry in the small- x region and is

consistent with the strange-to-down antiquark ratio $r_s = 1.00^{+0.25}_{-0.28}$ at $x = 0.023$ and $Q^2 = 1.9$ GeV² from ATLAS [17]. This is also consistent with the expectation that the extrinsic sea, which dominates at small x , is flavor independent.

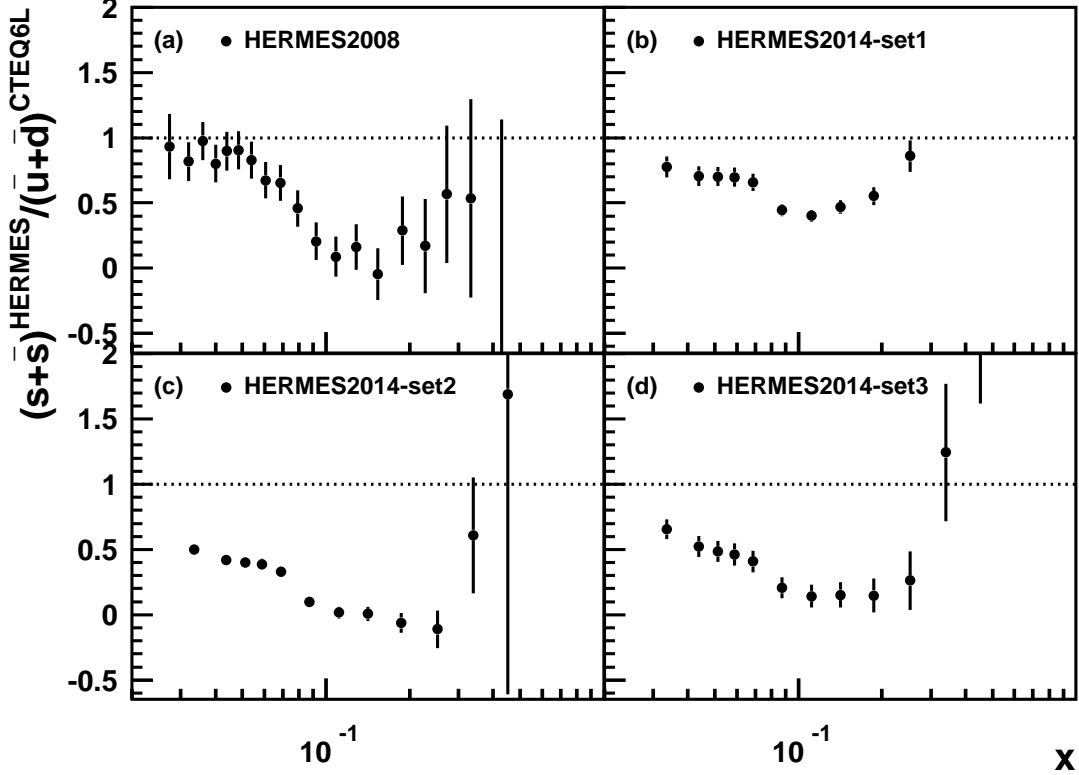


FIG. 5: The ratio of strange-to-nonstrange sea quarks $(s + \bar{s})/(\bar{u} + \bar{d})$ as a function of x . The $\bar{u}(x) + \bar{d}(x)$ is obtained from the CTEQ6L [15] PDF while the labels (a), (b), (c) and (d) denote the different input of $xS(x)$ from HERMES2008, HERMES2014-set1, HERMES2014-set2 and HERMES2014-set3, respectively.

V. SUMMARY

In summary, we have studied the implications of the latest HERMES data on the strange-quark content and the intrinsic light-quark sea in the proton. We show that the striking result of a vanishing $xS(x)$ at $x > 0.1$, reported as a favored solution by HERMES, is due to an assumption with a significant systematic uncertainty. We have calculated the five-quark components based on the BHPS model using the latest HERMES results on $xS(x)$. The new HERMES results affect the strange content quantitatively but do not exclude the existence of intrinsic light-quark component

in nucleon sea. The x dependence of the strange-to-nonstrange sea quark ratio, $(s + \bar{s})/(\bar{u} + \bar{d})$, is also in good qualitative agreement with the presence of both the extrinsic and the intrinsic seas in the proton. A reliable extraction of $xS(x)$ and the intrinsic strange quark sea calls for a more precise knowledge on the kaon fragmentation functions, and a new global fit taking into account the recent kaon SIDIS data.

This work was supported in part by the National Science Council of the Republic of China and the U.S. National Science Foundation.

-
- [1] J.P. Speth and A.W. Thomas, *Adv. Nucl. Phys.* **24** (1998) 83.
 - [2] S. Kumano, *Phys. Rep.* **303** (1998) 183.
 - [3] R. Vogt, *Prog. Part. Nucl. Phys.* **45** (2000) 105.
 - [4] G.T. Garvey and J.C. Peng, *Prog. Part. Nucl. Phys.* **47** (2001) 203.
 - [5] J.C. Peng and J.-W. Qiu, *Prog. Part. Nucl. Phys.* **76** (2014) 43.
 - [6] W.C. Chang and J.C. Peng, *Prog. Part. Nucl. Phys.* **79** (2014) 95.
 - [7] A. I. Signal and A. W. Thomas, *Phys. Lett. B* **191** (1987) 205.
 - [8] H. Holtmann, A. Szczurek and J. Speth, *Nucl. Phys. A* **596** (1996) 631.
 - [9] C. Bourrely, J. Soffer and F. Buccella, *Phys. Lett. B* **648** (2007) 39.
 - [10] R. S. Bhalerao, *Phys. Rev. C* **63** (2001) 025208.
 - [11] M. Wakamatsu, *Phys. Rev. D* **67** (2003) 034005; *Phys. Rev. D* **67** (2003) 034006; *Phys. Rev. D* **90** (2014) 034005.
 - [12] A. O. Bazarko *et al.* (CCFR Collaboration), *Z. Phys. C* **65** (1995) 189.
 - [13] O. Samoylov *et al.* (NOMAD Collaboration), *Nucl. Phys. B* **876** (2013) 339.
 - [14] A. Airapetian *et al.* (HERMES Collaboration), *Phys. Lett. B* **666** (2008) 446.
 - [15] J. Pumplin, D. R. Stump, J. Huston, H. L. Lai, P. M. Nadolsky and W. K. Tung, *JHEP* **07** (2002) 012.
 - [16] R. S. Towell *et al.* (NuSea Collaboration), *Phys. Rev. D* **64** (2001) 052002.
 - [17] G. Aad *et al.* (ATLAS Collaboration), *Phys. Rev. Lett.* **109** (2012) 012001.
 - [18] G. Aad *et al.* (ATLAS Collaboration), *JHEP* **1405** (2014) 068.
 - [19] S. J. Brodsky, P. Hoyer, C. Peterson and N. Sakai, *Phys. Lett. B* **93** (1980) 451; S. J. Brodsky, C. Peterson and N. Sakai, *Phys. Rev. D* **23** (1981) 2745.
 - [20] W. C. Chang and J. C. Peng, *Phys. Rev. Lett.* **106** (2011) 252002; *Phys. Lett. B* **704** (2011) 197.

- [21] P. M. Nadolsky, H. -L. Lai, Q. -H. Cao, J. Huston, J. Pumplin, D. Stump, W. -K. Tung and C. -P. Yuan, Phys. Rev. D **78** (2008) 013004.
- [22] A. Airapetian *et al.* (HERMES Collaboration), Phys. Rev. D **87** (2013) 074029.
- [23] A. Airapetian *et al.* (HERMES Collaboration), Phys. Rev. D **89** (2014) 097101.
- [24] D. de Florian, R. Sassot and M. Stratmann, Phys. Rev. D **75** (2007) 114010.
- [25] H. L. Lai, P. M. Nadolsky, J. Pumplin, D. Stump, W. K. Tung and C. -P. Yuan, JHEP **04** (2007) 089.
- [26] R. D. Ball, V. Bertone, S. Carrazza, C. S. Deans, L. Del Debbio, S. Forte, A. Guffanti and N. P. Hartland *et al.*, Nucl. Phys. B **867** (2013) 244.
- [27] L. A. Harland-Lang, A. D. Martin, P. Motylinski and R. S. Thorne, Eur. Phys. J. C **75** (2015) 5, 204.
- [28] M. Epele, R. Llubaroff, R. Sassot and M. Stratmann, Phys. Rev. D **86** (2012) 074028.
- [29] E. Seder (for COMPASS collaboration), DIS2015, 23rd International Workshop on Deep-Inelastic Scattering and Related Subjects , Dallas, 27 April-01 May, 2015; M. Stolarski (for COMPASS collaboration), SPIN2014, 21st International Symposium on Spin Physics, Beijing, 19-24 Oct, 2014.